Journal of Materials Chemistry B

Accepted Manuscript

ROYAL SOCIETY OF CHEMISTRY

www.rsc.org/materialsB

Journal Name

ARTICLE

Plasmon-induced Hyperthermia: Hybrid Upconversion $NaYF_4$:Yb/Er and Gold Nanomarterials for Oral Cancer Photothermal Therapy

Received 00th January 20xx,
Accepted 00th January 20xx

DOI: 10.1039/x0xx00000x

www.rsc.org/

Chieh-Wei Chen[a], Po-Han Lee[a], Yung-Chieh Chan[b], Michael Hsiao[b,d,], Chung-Hsuan Chen[b], Pin Chieh Wu[e], Pei Ru Wu[e], Din Pin Tsai[e,f,*], Datao Tu[g], Xueyuan Chen[g,*] and Ru-Shi Liu[a,b,c,*]*

Nanocomposites consisting of upconversion nanoparticles (UCPs) and plasmonic materials have been widely explored for bio-imaging and cancer photothermal therapy (PTT). However, several challenges, including incomprehensible efficiency of energy transfer processes and optimization of the conditions for plasmon-induced photothermal effect, still exist. In this study, we fabricated a $NaYF_4$:Yb^{3+}/Er^{3+} nanoparticles (NPs) conjugated with gold nanomaterials (Au NMs), such as Au NPs and gold nanorods (Au NRs). $NaYF_4$:Yb^{3+}/Er^{3+} NPs were used as a photoconverter, which could emit green and red light under exciting a 980 nm laser; Au NPs and Au NRs were also prepared and used as heat producers. Silica shell was further coated around UCPs to improve biocompatibility and as a bridge linking UCPs and the Au NMs. Most importantly, the thickness of the silica shell was tuned precisely to investigate the effective distance of plasmonic field for heat induction. Energy transfer was confirmed by the declining UCL photoluminescence and emission decay time after connecting to the Au NMs. Moreover, a simulative model was built by finite element method to assess the differences in heat generation between UCP@SiO_2-NP and UCP@SiO_2-NR. The surfaces of the hybrid nanocomposites were modified with folic acid to improve the specific targeting to cancer cells. The performance of the modified hybrid nanocomposites in PTT for OECM-1 oral cancer cells was evaluated.

1. Introduction

Hyperthermia is a type of physical treatment for cancer therapy that has been widely used with chemotherapy to improve therapeutic efficiency and prevent drug resistance.[1] To develop a high performance material for hyperthermia, the most important factors, such as effective therapy on tumor region and efficient use of energy, should be considered. Traditionally, gold nanomaterials (Au NMs) such as nanoparticles (Au NPs), nanorods (Au NRs), and nanoshells (Au NSs), are most commonly used for hyperthermia; not only their enhanced permeability and retention effect could let them passively accumulate in tumor environment, but their photothermal effect could also generate heat by direct laser irradiation.[2-4] Photothermal effect is a strong non-radiative process caused by the surface of electron that has a strong oscillation when Au NMs are irradiated with light. In this study, near-infrared (NIR) laser is used as a treating source because it has a maximum permeability at physiological organization and minimum affected quencher, such as water and hemoglobin in human body.[5] To date, theranostic (i.e., a combination of therapeutic and diagnostic) is the long-term goal in the development of personal nanomedicine; however, the Au NMs are difficult to apply directly in bio-imaging without further modification of other fluorescent dyes or other nanomaterials (NMs) and specific microscopy-like dark field and two-photon microscopy.[6-9] Therefore, convenient multifunctional NMs are necessary for cancer treatment.

In a method of combined photothermal therapy (PTT) and cell imaging, upconversion NPs (UCPs) are considered for use owing to their multi-emission in different regions, low excitation background, and long lifetime. UCPs have been developed for various applications, such as biosensor,[10, 11] water splitting,[12] photodynamic therapy[13] and gene delivery[14] because of their unique radiative process. UCPs consist of a host material (e.g., LaF_3, ZrO_2 and $NaYF_4$) doped with lanthanide ions (e.g., Yb^{3+}, Er^{3+} and Ho^{3+}) as sensitizer or activator. Basically, lanthanide ions are the core factors in upconversion systems because of the two following reasons: (1) all lanthanide ions have a considerable number of *4f* energy levels that are necessary for the upconversion process given that upconversion is a nonlinear process, which might absorb two or more photons and emit one photon with higher energy, such as UV, visible or NIR light.[15, 16] Emission color could also be tuned by doping different activators and the composition ratio of sensitizer and activator. Furthermore, Yb^{3+}, which is a commonly used sensitizer, has large absorption cross-section at 980 nm.[17] (2) The electron could easily transfer to neighboring levels because most energy levels are close with one another. However, the efficiency of upconversion process is still a key problem because the nature of *4f–4f* electronic transitions are Laporte forbidden.[18] Therefore, many researchers have tried to enhance photoluminescence (PL) intensity through

coating an inner or active shell with similar crystalline material around the surface of UCPs to reduce the surface defect and interference by solvent quencher from non-radiative decay.[19] An active shell could further enhance the PL than an inner shell because the pumping photons will increase by co-doping a sensitizer in the core and outer shell.[20] UCPs coupled with plasmonic materials (e.g., Au NMs and Ag NMs) have also exhibited enhanced PL through surface-plasmon-coupled emission (SPCE) or local field enhancement effect by increasing the emission rate or the excitation rate, respectively.[21-24]

Moreover, plasmonic materials could be directly used as heat generators because of their photothermal effect. In a hybrid UCPs and plasmonic material system, the energy source for the PTT application could be an external laser or the UCPs. For the hybrid UCPs, Cheng and co-workers fabricated nanocomposites consisting of UCPs and iron oxide NPs which were covered with Au NS and then applied for cancer cell magnetic resonance imaging and PTT.[25] The SPR absorption peak red-shifted after Au NPs aggregation, which is similar to that for the Au NS. After the Au NS formation, the SPR peak slightly red-shifted, and another absorption band becomes obvious at the NIR region. Therefore, individual 980 and 808 nm laser should be used for excitation in cancer cell upconversion luminescence (UCL) imaging and PTT, respectively. Moreover, Dong *et al.* fabricated $NaYF_4$:Yb^{3+}/Er^{3+}@Ag core/shell nanocomposites and used for PTT by exciting one 980 nm laser because Ag NS could tune the SPR peak to 980 nm.[26] However, fully coated outer shell formed by plasmonic NMs might cause unfavorable influence, in which not only the excitation light may be scattered, but also the UCP absorption efficiency may be decreased and the emission intensity may even be intensely quenched.[22] For the plasmonic material system, heat is produced through luminescence resonance emission transfer (LRET) from UCPs to Au NMs. Qian *et al.* used a reverse micro-emulsion process to prepare hybrid nanocomposites, in which Au NPs are directly decorated on the surface of the silica shell. However, only a 4 °C difference was found between the heating performance of $NaYF_4$:Yb^{3+}/Er^{3+}@SiO_2-Au NPs, and $NaYF_4$@SiO_2-Au NPs.[27] Moreover, Song and co-workers constructed a unique Au NP@UCP core/shell structure, which has the potential for PTT application, but they only examined the temperature changes and confirmed that energy could be transferred to Au core via a decreasing in UCL emission.[28] Both systems have no complete results to verify the optimized conditions for nanoplatform application in cancer cell PTT with good performance, such as (1) confirmation of the energy transfer by other evidence, (2) the distance between UCPs and Au NMs that could exert high efficiency of photothermal effect by plasmonic field, and (3) the amount of Au NM loading that could give sufficient heat for PTT without quenching the UCL intensity.

In the present study, we fabricated multifunctional nanocomposites based on the conjugating upconversion of $NaYF_4$:Yb^{3+}/Er^{3+} NPs and Au NPs or Au NRs through the combination of unique multi-emission and SPR effect for oral cancer PTT. We tried to evaluate which Au NMs have high potential of absorbing the energy from UCPs by photothermal effect in terms of the difference in SPR absorption peak. UCPs were coated with silica shell (with different thickness) to investigate the affected range of plasmonic field, and Au NMs were directly decorated on silica shell by electronic force. To improve the targeting ability, the silica shell was modified with folic acid (FA) by NHS/EDC coupling reaction. We also used a simulative model to study the dissimilitude between Au NPs and Au NRs with regard to generation of heat under irradiation of the individual emission bands. Results showed that UCP@SiO_2-NRs-FA has higher quality for heat production than UCP@SiO_2-NPs-FA. The modified hybrid nanocomposites also exhibited an effective ability for cancer cell PTT and imaging.

2. Experimental

Chemicals and materials

Chloroauric acid, silver nitrate, citric acid, ascorbic acid, and CTAB were purchased from Acros. Ammonium solution (28%–30%) was purchased from J.T. Baker. $Y(CH_3CO_2)_3{\cdot}xH_2O$ (99.9%), $Yb(CH_3CO_2)_3{\cdot}4H_2O$ (99.9%), $Er(CH_3CO_2)_3{\cdot}xH_2O$ (99.9%), NaOH (98+%), NH_4F (98+%), 1-octadecene (90%), OA (90%), IGEPAL® CO-520, TEOS (98%), APTES (98%), N-hydroxysuccinimide (NHS), N-(3-Dimethylaminopropyl)-N-ethylcarbodiimide hydrochloride (EDC), chitosan (low molecular weight, 99%), monochloroacetic acid (≥99.0%), sodium borohydrideand (≥99.0%) and FA were purchased from Sigma-Aldrich. 4',6-Diamidino-2-phenylindole (DAPI) was purchased from InvitrogenTM. Deionized water was obtained using a Milli-Q SP ultrapure-water purification system from Nihon Millipore Ltd., Tokyo. All chemicals were used as received without further purification.

Synthesis of $NaYF_4$:Yb^{3+}/Er^{3+} NPs

$NaYF_4$:Yb,Er NPs were synthesized via a modified high temperature co-precipitation method according to a literature procedure.[29] $Y(CH_3CO_2)_3{\cdot}xH_2O$ (85.13 mg; 0.32 mmol), $Yb(CH_3CO_2)_3{\cdot}4H_2O$ (25.21 mg; 0.072 mmol), and $Er(CH_3CO_2)_3{\cdot}xH_2O$ (5.51 mg; 0.008 mmol) were added into 50 mL two-neck round-bottom flask with OA (3 mL) and 1-octadecene (7 mL). The solution was heated to 150 °C under the protection of nitrogen for 30 min to dissolve the lanthanide salts and cooled down to 50 °C. Subsequently, a methanol solution (3.0 mL) containing NH_4F (59.26 g; 1.6 mmol) and NaOH (0.04 g; 1.0 mmol) was added and stirred for 30 min. The reaction mixture was then heated at 100 °C for 30 min to remove the methanol; the solution was then heated to 290 °C and kept for 2 h before cooling to room temperature. The as-prepared NPs were precipitated by adding absolute ethanol, collected by centrifugation at 6000 rpm for 10 min, and washed with ethanol for several times. The UCPs were stored in cyclohexane for the next step.

Synthesis of UCP@SiO_2-NH_2

Silica shells were coated on the UCPs and further functionalized with amino groups through a reverse micro-emulsion.[30] Approximately 1 mL of CO-520 was dispersed in 10 mL of cyclohexane for 30 min stirring. Afterwards, approximately 10 mg of UCPs were prepared in 1 mL of cyclohexane solution and added into the mixture for 1 h. Approximately 0.1 mL of ammonium solution was added for another 1 h. Afterwards, different amounts of TEOS were slowly added using a syringe pump to control the flow rate in 400 μL/h, and the reaction was gently stirred for 24 h. The thicknesses of silica shell as 1.2, 2.2, 4.3, 7.9 and 12.9 nm could be tuned by adding 10, 20, 40, 80 and 100 μL, respectively. To graft amino groups on the surface, approximately 0.1 mL APTES was slowly injected into the system, and stirring was kept for another 4 h. The product could be precipitated by adding methanol and collected by centrifugation (7800 rpm, 20 min). After several washing by MeOH, UCP@SiO_2-NH_2 was finally dispersed in deionized water or EtOH.

Synthesis of UCP@SiO_2-NPs-FA and UCP@SiO_2-NRs-FA

The 3.5 nm Au NPs were synthesized using a typical method that used $NaBH_4$ as a strong reduction agent and citric acid as a capping ligand; Au NRs were prepared, and the SPR absorption peak of Au NRs were adjusted to match the UCL emission via a modified seed-mediated growth method.[31] FA was then modified on the

UCP@SiO_2 through NHS/EDC coupling reaction.[32] Briefly, FA, NHS and EDC were mixed for activation in a molar ratio of 1:2.5:1 (1.2, 3 and 1.2 μmol) for 1 h at RT. Afterwards, approximately 10 mg of UCPs@SiO_2-NH_2 were added to the mixture solution to react for another 12 h at RT. UCP@SiO_2-FA was purified with EtOH by centrifugation (12000 rpm, 12 min). The obtained product UCP@SiO_2-FA could be dispersed into water or buffer solution for a long time with high stability. Before Au NPs and Au NRs were decorated on the UCP@SiO_2-FA, both Au NPs and Au NRs exchanged the surface ligand to OCMCS. This process was directly added with 0.5 mg/mL OCMCS in the NPs solution and stirred for at least 12 h. The CTAB concentration in Au NRs solution should be washed by water until lower than 500 μM because the long chain from CTAB discouraged the ligand exchange reaction. UCP@SiO_2-NPs-FA or UCP@SiO_2-NRs-FA were then obtained from the different volumes of Au NPs or Au NRs reacting with UCP@SiO_2-FA for 1 h. The products were then purified through centrifugation (10000 or 5000 rpm for NP or NR system, respectively).

Photothermal ability of UCP@SiO_2-NP or UCP@SiO_2-NR in solution

To test the photothermal conversion for nanocomposites, approximately 200 μL of UCP@SiO_2-NP or UCP@SiO_2-NR (1 mg/mL for each sample) were prepared in the water, and the samples were placed in the quartz cuvette by directly irradiating 1.5 W/cm^2 at 980 nm laser for 3 min. The variation in temperature will be recorded by thermocouple every 10 sec.

Simulative analysis

All the simulated spectra and field distributions were obtained by solving three-dimensional Maxwell equations with FEM. The permittivity of gold is described by Drude–Lorentz model with plasmon frequency of ωp = 8.997 eV and damping constant of Γp = 0.07 eV. The refractive index of water, UCPs, and SiO_2 is fixed at 1.33, 1.8 and 1.46, respectively. An electric dipole source with current amplitude of 1 A/m $\left(\vec{I} = (\frac{1}{\sqrt{3}}\hat{\imath} + \frac{1}{\sqrt{3}}\hat{\jmath} + \frac{1}{\sqrt{3}}\hat{k})\right)$, where $\hat{\imath}$, $\hat{\jmath}$ and $\hat{k}$ is the unit vector along x-, y- and z-axis, respectively) is used to simulate the light emitted from UCP. The scattering boundary condition is used to avoid the reflection influence. According to the UCP experimental spectra, three peak wavelengths (525, 540 and 655 nm) were employed for the induced heat study. The total number of photons emitted from UCPs was realized by measuring the laser power and the quantum yield of UCPs. According to the emission spectra, the power of the emitted light from UCPs in λ = 525, 540 and 655 nm is 17, 67 and 21 W/m^2, respectively. The time average resistive heating Qave can be obtained by calculating the time average resistive heating,[33] which is defined as follows:

$$\boldsymbol{Q_{ave}} = \frac{\mathbf{1}}{\mathbf{2}}\boldsymbol{Re}\left(\boldsymbol{\sigma}\,\vec{\boldsymbol{E}}\cdot\vec{\boldsymbol{E}}^{*} - \boldsymbol{j\omega}\vec{\boldsymbol{E}}\cdot\vec{\boldsymbol{D}}^{*}\right)$$

where E is the electric field, D is the electric displacement field, and ω is the angular frequency. The induced heat is subsequently calculated by integrating the resistive heating on gold particles.

Cell viability assay and cellular uptake

The cell viability assay was applied on OECM-1 oral cancer cells treated with UCP@SiO_2, UCP@SiO_2-NP-FA, and UCP@SiO_2-NR-FA for 24 and 72 h. OECM-1 cell lines were cultured in an incubator under 37 °C and 5% CO_2 using the typical method, and the cell medium used was RPMI-1640 medium mixed with 10% fetal bovine serum and penicillin/streptomycin L-glutamine. For the 24 h treatment, approximately 2000/mL cells were loaded in each 96-well plates for 12 hours. Various concentrations of nanocomposites (1, 3, 9, 27, 81 and 250 μg/mL) were then added to the plates and incubated for 24 h. For the 72 h treatment, the cell number will also use 2000/mL cells to prevent cell overgrowth, which can lead to dead or unhealthy cells. The resulting cell viability was calculated via an Alamar Blue assay using 560 EX nm/590 EM nm filter settings to determine the fluorescence intensity.

In vitro confocal images were obtained using a Leica TCS SP5 confocal microscopy. Oral cancer cells (OECM-1) were incubated with UCP@SiO_2, UCP@SiO_2-NPs-FA, and UCP@SiO_2-NRs-FA for 12 h in 6-well plates at 37 °C in a 5% CO_2 humidity atmosphere. All of the cells were incubated on top of cover glass. The samples on the slides for capturing confocal images were prepared in several steps. Briefly, the culture medium was vacuumed to remove the free nanocomposites. Exponentially growing cells were fixed on the piece of cover glass using 4% paraformaldehyde, 1 mL per well for 5 min. The nuclei in the cultures were stained with DAPI for a further 5 min to label the cells. After the staining procedure, the pieces of the cover glasses were stuck on the top of the slides with moderate mounting oil between them. Nuclei image was obtained by exciting an ultraviolet laser at 360 nm, and the emission was detected between 450-470 nm; UCP images were excited in an NIR laser at 980 nm, and the emission was detected between 500-560 nm.

PTT test

In the photothermal ablation experiment, the OECM-1 oral cancer cells were loaded in 12-well plates, and approximately 100 μg/mL were treated with low and high Au/Y ratio of UCP@SiO_2-NP-FA and UCP@SiO_2-NR-FA for 12 h (UCP@SiO_2, Au NPs and Au NRs as the control group, and both Au NMs of the concentrations were 100 mg/mL). After the treatment, the nanocomposites were removed by PBS buffer (pH 7.4). Following incubation for 12 h in an incubator, the target cells were irradiated with 1.5 W/cm^2 by a NIR laser at a 980 nm wavelength for 1 min. Trypan blue, a dye that is commonly used to color dead tissues or cells blue selectively, was added to the cell dishes for 30 min.

Characterizaion

The morphology of the samples was studied using TEM, with an electron gun operating at 100 keV. The TEM and HRTEM images were collected using a JEOL JEM-2100F electron microscope, and the crystalline phase of UCPs was characterized by 1.54 Å XRD pattern (Bruker D_2 phaser diffractometer). The UCL emission spectra of samples were detected by a PL system with excitation at 980 nm. The zeta potential of UCP@SiO_2 and UCP@SiO_2-NH_2 was measured by MALVERN ZETASIZER-3000 at room temperature in EtOH. The UV/Vis absorption spectra of the colloidal solution of Au NPs and Au NRs were obtained at room temperature using a SHIMADZU UV-700 spectrophotometer with a 1 cm wide quartz cuvette at room temperature. Meanwhile, the FT-IR spectra of UCPs and UCP@SiO_2, which were dispersed in KBr pellets, were obtained using a Varian FTIR-640 spectrometer. The gold concentration in the as-prepared colloid solution was determined using ICP-MS. The sample was investigated using confocal microscopy (Leica TCS SP_2 AOBS) for the internalization efficiency of the NMs and the PTT test. UC PL lifetimes were measured with a customized UV to mid-infrared steady-state and phosphorescence lifetime spectrometer (FSP920-C, Edinburgh Instrument) equipped with a digital oscilloscope (TDS3052B, Tektronix) and a tunable mid-band optical parametric oscillator pulse laser as the excitation source (410-2400 nm, 10 Hz, pulse width ~5 ns, Vibrant 355II, OPOTEK).

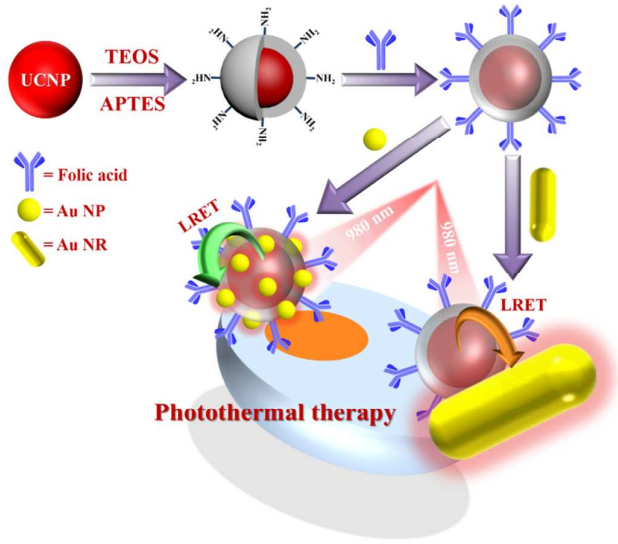

Scheme 1. Schematic illustration for synthetic process of UCP@SiO_2-NPs and UCP@SiO_2-NRs and applying in oral cancer cell PTT.

3. Results and discussion

Characterization of UCP@SiO_2-NPs-FA and UCP@SiO_2-NRs-FA

Scheme 1 shows the preparation process of the nanocomposites UCP@SiO_2-NPs-FA and UCP@SiO_2-NRs-FA and their application to OCEM-1 oral cancer cells. Au NMs were decorated on the UCP@SiO_2 after FA modification because of the reaction involving the NHS/EDC coupling reaction, which would affect the stability of Au NMs or cause aggregation. First, $NaYF_4$:Yb^{3+}/Er^{3+} NPs were synthesized through a high-temperature co-precipitation method with capping reagent of oleic acid (OA) in octadecene;[29] the average diameter of the $NaYF_4$:Yb^{3+}/Er^{3+} NPs was approximately 20.6 ± 1.5 nm and their morphology showed a uniform sphere without aggregation. The transmission electron microscopy (TEM) image of $NaYF_4$:Yb^{3+}/Er^{3+} NPs is shown in Figure 1a. Moreover, silica shells were coated around the UCPs by a modified reverse water-in-oil micro-emulsion procedure,[34] and 3-aminopropyl-triethoxysilane (APTES) was used to extend the amino group on the surface of silica to connect to Au NPs or Au NRs. In this process, the zeta potential of UCP@SiO_2-NH_2 would change from ζ = −28 to ζ = +23, which proved that the amino group was grafted on the surface. The thickness of silica shell could be easily controlled at 1.2, 2.2, 4.3, 7.9 and 12.8 nm via reaction with increased amount of tetraethyl orthosilicate (TEOS) (Figure S1). Meanwhile, Fourier transform infrared (FT-IR) spectroscopy was used to confirm the silica shell modification. For UCPs capped with OA, the stretching bands of 2935 and 2859 cm^{-1} indicated a C–H stretching vibration, and 1566 and 2859 cm^{-1} were assigned to a COO^- stretching vibration. After silica shell modification, the strong stretching vibrations of 3465 and 1080 m^{-1} were expressed as O–H and Si–O–Si, respectively (Figure S2). The crystalline phase of the $NaYF_4$:Yb^{3+}/Er^{3+} NPs was confirmed as hexagonal according to the reference peak (JCPDS file no. 16-0334). The high-resolution TEM image also showed a lattice fringe of approximately 0.29 nm, which was denoted to be the (101) phase in hexagonal crystalline by powder X-ray diffraction (XRD) (Figures 1b-1c). In UCP systems, $NaYF_4$ is one of most commonly used host materials in the upconversion process because of its low non-radiative loss and the ion radius of Y^{3+} is similar to that of trivalent ion of lanthanide. Moreover, Yb^{3+} could sufficiently absorb the energy denoted to 980 nm light because of its 4f level transition of $^2F_{7/2} \rightarrow {}^2F_{5/2}$. Er^{3+} was doped to obtain UCLs at 408, 521, 541 and 654 nm, which are attributed to $^2H_{9/2} \rightarrow {}^4I_{15/2}$, $^2H_{11/2} \rightarrow {}^4I_{15/2}$, $^4S_{3/2} \rightarrow {}^4I_{15/2}$ and $^4F_{9/2} \rightarrow {}^4I_{15/2}$ transitions, respectively. After silica shell coating, the PL intensity decreased by 25% because of the change in dielectric constant (Figure 1d).

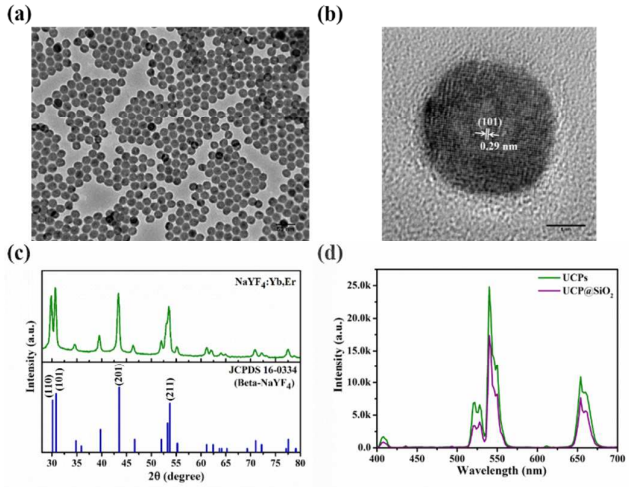

Figure 1. Characterization of $NaYF_4$:Yb^{3+}/Er^{3+} NPs: a) TEM image, b) HRTEM image and c) crystalline phase of $NaYF_4$:Yb^{3+}/Er^{3+} NPs; d) UCL emission before and after coating with 4.3 nm of silica shell.

To determine the optimal conditions for UCP@SiO_2-Au NMs-FA application for PTT and cell imaging, a balanced point for UCL quenching and enhancing should be established, including the effective modification amount of Au NMs and the thickness of silica shell. Furthermore, the SPR absorption peak of Au NRs should be adjusted at first to match the UCL emission because the 3.5 nm Au NPs already revealed a strong SPR at approximately 525 nm. We tuned the SPR position of Au NRs by adding less silver nitrate during the growth reaction because silver ions play as active sites. Therefore, less silver ions could cause short Au NRs, and thus the SPR was tuned at 525 and 655 nm.[31] However, a typical seed-mediated growth method for Au NRs synthesis involves a high-cytotoxicity surfactant, such as hexadecyltrimethylammonium bromide (CTAB).[31] To reduce the latent hazard of cytotoxicity for Au NRs from CTAB and adjust the surface charge to negative, CTAB should be exchanged with O-carboxymethylchitosan (OCMCS) in Au NRs. Both Au NPs and Au NRs replaced the protecting ligands by OCMCS and showed the same surface property. OCMCS, which has high biocompatibility and could stabilize Au NMs in solution, were prepared in the same method from our previous report.[35] Subsequently, different volumes of Au NPs and Au NRs would individually react with various thicknesses of UCP@SiO_2, enabling further study of the influence of SPR effect. Moreover, the precise Au/Y ratio would be detected by inductively coupled plasma mass spectrometry (ICP-MS). In Figure 2, the emissions of UCL at 521 and 654 nm for UCP@SiO_2-NPs and UCP@SiO_2-NRs were different. For UCP@SiO_2-NPs, when the silica shell was 1.2 nm thick, the PL intensity decreases by 25% or 50% at 521 nm with 0.86 and 1.42 Au/Y ratios, respectively, and the PL intensity only slight change when the silica shell thickness increases, except for the 1.42 Au/Y ratio. Meanwhile, for UCP@SiO_2-NRs, both emissions at 521 and 654 nm vary with different Au NR loadings and silica shell thickness. At low loading of Au NRs as 0.21 and 0.84 Au/Y ratios, the UCL

intensity could be enhanced by approximately 1.25 or 1.5 times when the silica shell thickness was below 10 nm and decline in all thickness values for 1.41 and 2.59 Au/Y ratios. The conditions for emission at 408 and 541 nm were similar to that at 521 nm, as shown in Figure S3. Consequently, the SPR effect was the main factor that affects UCL intensity because the noticeably enhanced or quench phenomena could only be observed in UCP@SiO_2-NRs. Also, the UCL intensity will be affected by the interaction between the excitation light (980 nm laser) and coupling effect from Au NRs, because some of Au NRs would be close to each other in random and generate a region with high density of electron (hot spot), which could potentially cause influence of UCL by interacting with light source.[24] However, this phenomena would only result from the case of Au NRs, because the wavelength of laser source could not affect with Au NPs.

The minor factor would be the amount of Au NMs; that is, UCL would be increased with low amount of Au NMs. Moreover, silica shell was the least factor that influences UCL because the average intensity had no dramatic change. Figure 3 shows the diversity of SPR effect from Au NPs and Au NRs influencing UCL. The Au NPs can only generate one plasmonic field by exciting the green emission (521 and 541 nm) from the UCPs, but the Au NRs could create two plasmonic fields by exciting both green and red emissions (521, 541 and 654 nm), which would match to induce strong oscillation of surface electron. In general, the emission intensity would be first quenched because the energy absorbed by Au NMs under certain critical situation could further improve the irradiative process through SPCE effect.[36] For UCP@SiO_2-NPs, this phenomenon explained that some UCLs present declining or similar intensities because of the weak interaction from plasmonic enhancement. Moreover, when the Au/Y ratio increased to a high density of cover layer on the UCP@SiO_2, the absorption efficiency to UCPs at 980 nm is interrupted and the emission from UCPs is hindered.[22]

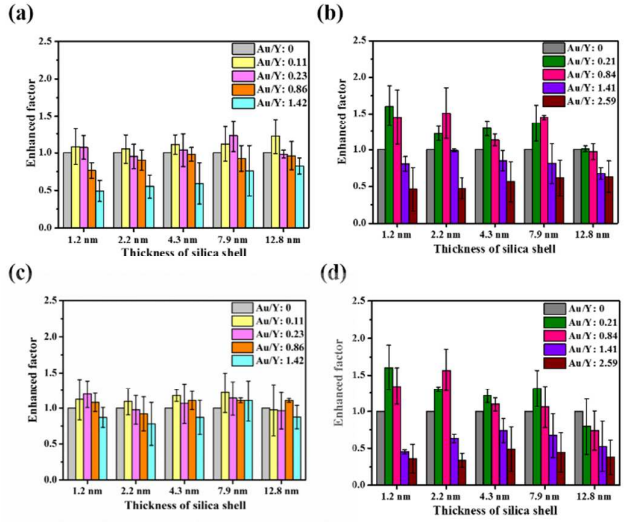

Figure 2. Different Au/Y ratio of UCL emission for UCP@SiO_2-NPs at a) 521 nm and c) 654 nm; UCP@SiO_2-NRs b) 521 nm and d) 654 nm.

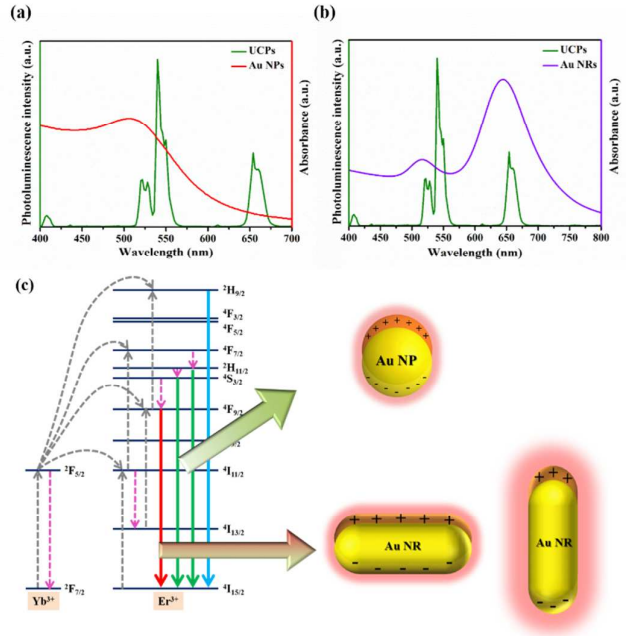

Figure 3. Overlapping diagram of UCL emission and absorption of a) Au NPs and b) Au NRs; c) Schematic diagram of Mechanism for upconversion process and energy transfer for Au NPs or Au NRs inducing heat, repoectively.

To apply UCP@SiO_2-NPs and UCP@SiO_2-NRs for PTT, the energy must be sufficiently absorbed by Au NMs because the photothermal effect induces a heating process from a non-radiative oscillation from the surface of electrons. Therefore, the high quantity of Au NMs was a main factor because of the obvious decrease in UCL intensity, which implied an effective energy transfer to Au NMs. In Figure 4, we considered the Au/Y ratios of 0.84 and 1.41 for UCP@SiO_2-NRs (0.86 and 1.42 Au/Y ratios for UCP@SiO_2-NPs) that could present a low and high loading amount for investigation of the photothermal property without fully quenching the UCL intensity. Moreover, 1.2 and 4.3 nm thick silica shells were also used to determine the influence of distance spacer; these two thicknesses were referred to as near and far distance for investigation. To verify the efficiency of transferring light to heat energy, we performed a simple test, in which the temperature of the solution was monitored during irradiation by a 980 nm laser. In Figure 5, the silica shells are 1.2 and 4.3 nm thick; in both results, the temperature rapidly increased within 40 sec, which slowly decreased with the proportion of growth. For 1.2 nm thickness, only UCP@SiO_2-NRs with a 1.41 Au/Y ratio could reach 52 °C. The other samples reached only 36-38 °C, except for water with almost no change, which might be caused by the unfavorable energy transfer during photothermal conversion. Based on Figure 4, only UCP@SiO_2-NRs with a 1.41 Au/Y ratio decreased considerably without enhancement of the UCL intensity. The same result is found for 4.3 nm thick silica shell, in which the obvious difference was caused by the enhanced or quenched UCL emission. The highest temperature was only 43.2 °C for 4.3 nm thick silica shells, and a lower rate of decline was observed for 1.2 nm thick silica shells. Thus, we suggest that heating process was the major exhibition under declining UCL emission. To investigate the different efficiencies of conversion for light to heat by Au NPs and Au NRs, the integrated areas of UCL emission spectra were compared with the individual

systems, which decreased by 33% and 45% after modifying Au NPs and Au NRs, respectively (Figure S4). This result provides an evidence for relatively high energy transfer to heat depending on the SPR absorption.

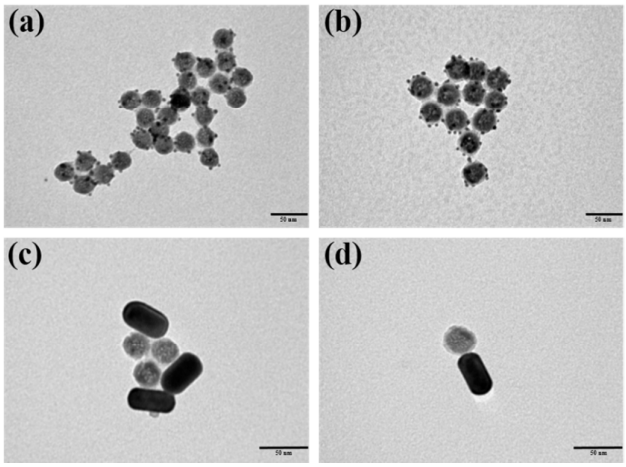

Figure 4. TEM images of UCP@SiO_2 conjugating with Au NPs: a,b) silica shell of 1.2 and 4.3 nm, and with Au NRs: c,d) silica shell of 1.2 and 4.3 nm.

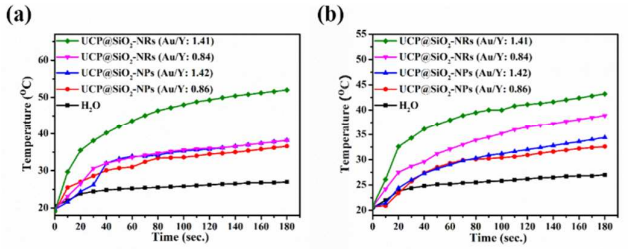

Figure 5. Photothermal ability for UCP@SiO_2-NPs and UCP@SiO_2-NRs as silica shell of a) 1.2 and b) 4.3 nm under irradiating 980 nm laser with 1.8 W/cm^2.

The emission decay time of the two types of nanocomposites were also measured at 541 and 654 nm, as shown in Figure 6. At 541 nm, both systems had a decreased PL lifetime after combining with Au NMs; moreover, the PL lifetime decreased from 94 μs to 75.2 and 85.1 μs when the Au/Y ratio was 1.41 and 1.42 for UCP@SiO_2-NPs and UCP@SiO_2-NRs, respectively. At 654 nm, the PL lifetime of the UCP@SiO_2-NRs declined from 249 μs to 167.8 μs with the increase in Au/Y ratio; conversely, the PL lifetime had almost similar values with UCP@SiO_2-NPs, from 249 μs to 245 μs. The decline in UCL intensity and PL lifetime might explain the energy transfer mechanism, as shown in Figure 3, in which the photon could be absorbed specifically through LRET to Au NMs, and this energy was used to generate heat by a non-radiative process.[37]

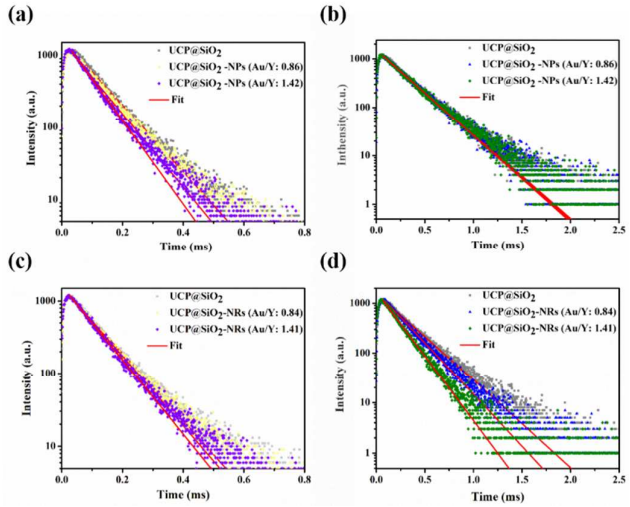

Figure 6. UCL emission decay time at a,c) 541 and b,d) 654 nm for UCP@SiO_2-NPs and UCP@SiO_2-NRs with different Au/Y ratio.

Simulative model for the evaluation of the heating variation

According to the optical characterization and photothermal test, UCP@SiO_2-NRs could possess a higher heating than UCP@SiO_2-NPs because energy was strongly absorbed from three emission bands, which were denoted at 521, 541 and 654 nm. However, the relationship between plasmonic field and heat quality was still unclear. To determine the basic variation of performance at different wavelength peaks for Au NPs and Au NRs, we used a simulative model built by finite element method (FEM) for a theoretical study. As shown in Figures 7 and 8, we fabricated a model consisted of UCP@SiO_2 and one Au NP or Au NR, and plasmonic field was generated under three emissions at 525, 540 and 655 nm. Moreover, to apply these nanocomposites as bifunctional NMs in PTT and cell imaging, 4.3 nm thick silica shells were selected for simulative study because of the absence of full UCL emission quenching at high Au/Y ratio. Figure S5 shows the distribution of electric field, which was derived to heat distribution by the time average resistive heating equation. The induced heat was subsequently calculated by integrating the resistive heating on Au NMs. The heat was also produced, depending on the SPR peak of Au NMs (Figures 7b-8b), For UCP@SiO_2-NP, heat could be noticeably generated at green emission only, which indicated the $^2H_{11/2} \rightarrow {}^4I_{15/2}$ and $^4S_{3/2} \rightarrow {}^4I_{15/2}$ transitions. The quality of heat was integrated in the whole area displayed on the Au NPs, which were 1.55×10^{-14}, 4.83×10^{-14} and 1.17×10^{-15} W at 525, 540 and 655 nm, and the difference between the heat quality at 540 nm and at 525 nm could be observed to be slightly three times more and almost 41 times than that at 655 nm ($^4F_{9/2} \rightarrow {}^4I_{15/2}$ transition) (Figure 7c). Moreover, two factors should be considered for the Au NRs, including SPR position and orientation of the connecting point, because the Au NRs are anisotropic NMs. For UCP@SiO_2-NR, we discussed the two major directions connecting at head or body of Au NR (x or y-axis), which the heat were 1.66×10^{-13}, 5.92×10^{-13} and 4.54×10^{-13} W for x axis, and 2.53×10^{-13}, 8.92×10^{-13} and 5.24×10^{-13} W for y axis at 525, 540 and 655 nm. (As shown in Figure 8c-8d) Also, the heat distribution at 655 nm was higher by 5.74 and 1.67 times than that at 525 nm and 540 nm, respectively, for the modification at x-axis; conversely, heat at 540 nm was higher by 3.53 and 1.6 times than that at 525 nm and 655 nm for y-axis, respectively. We accumulated all the integrated heat, including 525,

540 and 655 nm, and found almost the same values as 1.69×10^{-12} W and 1.67×10^{-12} W for the x-axis and y-axis of the connecting point. This phenomenon can be explained by Figure 8b, in which the total heat value calculated from the two bands (green and red) was similar around 40 fW. $NaYF_4$:Yb^{3+}/Er^{3+} NPs could also emit stronger green emission than red; when Au NR was conjugated with UCPs at y-axis, the efficient oscillations of electric field from green light absorption ($^2H_{11/2} \rightarrow {}^4I_{15/2}$ and $^4S_{3/2} \rightarrow {}^4I_{15/2}$) were the major affected radiation in heat production. However, when Au NR conjugated with UCPs by head point, red emission ($^4F_{9/2} \rightarrow {}^4I_{15/2}$) could be the major induced heat of radiation. This variation resulted in the strong heating process at weak red emission region, which corresponded to the high SPR absorption peak (655 nm). Meanwhile, comparison of the total integrated heat between the Au NP and Au NR systems showed that the UCP@SiO_2-NRs could efficiently generate more heat than the UCP@SiO_2-NPs by almost 26 times because better interaction between SPR and UCL existed in the former.

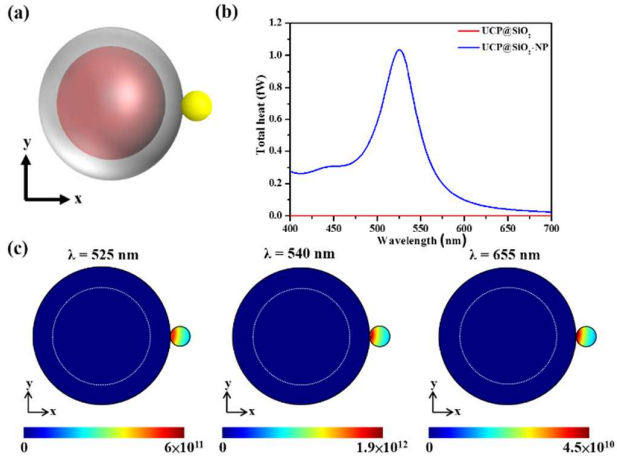

Figure 7. Simulative model for UCP@SiO_2-NP: (a) schematic construction of UCP@SiO_2-NP; (b) inducing heat from the construction of (a); (c) quality and distribution of heat on Au NP under irradiation of individual UCL emission at 525, 540 and 655 nm.

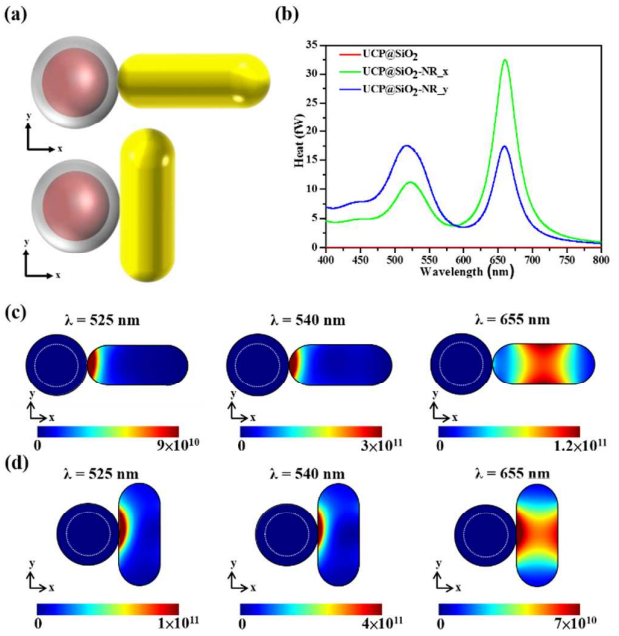

Figure 8. Simulative model for UCP@SiO_2-NR: a) schematic construction of UCP@SiO_2-NR; b) inducing heat from construction of a); quality and distribution of heat on Au NR under irradiation of individual UCL emission at 525, 540 and 655 nm for c) x axis and d) y axis.

UCP@SiO_2-NPs-FA and UCP@SiO_2-NRs-FA for PTT in vitro

According to the chemical, physical and theoretical characterization, the most suitable nanocomposite for oral cancer PTT between conjugating to Au NPs or Au NRs is the UCP@SiO_2-NRs because of the predominant performance of photothermal energy transfer. Moreover, the FA molecules were covalently bonded with $-NH_2$ on the silica surface to improve the targeting ability for cancer cells and the stability in the aqueous solution. In this study, we selected OECM-1 oral cancer cells to demonstrate PTT efficiency. OECM-1 is a kind of oral epidermoid carcinoma cell line. PTT treatment is better than chemotherapy because the latter has significant side effect and challenge. To eliminate the cytotoxicity of these nanocomposites to OECM-1 without laser treatment, we first incubated different concentrations of nanocomposites with OECM-1 for 24 and 72 h. In Figures 9a-9b, no obvious cytotoxicity was observed for UCP@SiO_2-FA; also after modification with Au NMs, the cell viability still remained above 90%, and the nanocomposite concentration was increased from 1 to 250 μg/mL in both 24 and 72 h treatment. Moreover, FA has been widely used for improving the intracellular uptake through caveolin-mediated endocytosis, and confocal microscopy was used to verify the effect FA modification in improving the binding affinity to cancer cells.[38, 39] As shown in Figure 9c, UCP@SiO_2-NRs-FA are highly accumulated into OCEM-1 and most of the nanocomposites are located around nuclei because they are too large to enter into the nuclei. Moreover, the improvement in accumulation could be attributed not only by FA modification but also by the adverse interaction between nanocomposites and OECM-1 because the zeta potential of these nanocomposites and the cell membrane were both negative. We then examined the therapeutic efficiency of both UCP@SiO_2-NPs-FA and UCP@SiO_2-NRs-FA with low and high loading amount of Au NMs via irradiation at 980 nm laser with 1.5 W/cm^2 (conservative limit set for human skin exposure to 980-nm NIR light is 0.7 W/cm^2,

ANSI Z136 Standards, http://www.lia.org/publications/ansi) for 1 min. Trypan blue was immediately used to stain the treated cell for quick PT efficiency test. In Figure 10, OECM-1 oral cancer cells were killed and a considerable difference was found between UCP@SiO_2-NPs-FA and UCP@SiO_2-NRs-FA, which is attributed to the discrepancy of heating ability and heat distribution. According to the simulative results from Figures 7 and 8, most of the heat was generated at the contact surface between the UCPs and the Au NMs, but the Au NRs could reveal preferable heating area because of their unique anisotropic property and large surface area. The Au NPs, Au NR and UCP@SiO_2 were also treated with OECM-1 for the control group, and the result showed no observable cell death after irradiation with a 980 nm laser (Figure S6). Compared with the UCP@SiO_2-NPs-FA with weak therapeutic performance, most of the cells were dead in UCP@SiO_2-NRs-FA treatment with a 1.41 Au/Y ratio, which showed excellent potential for PTT in OECM-1 oral cancer cells.

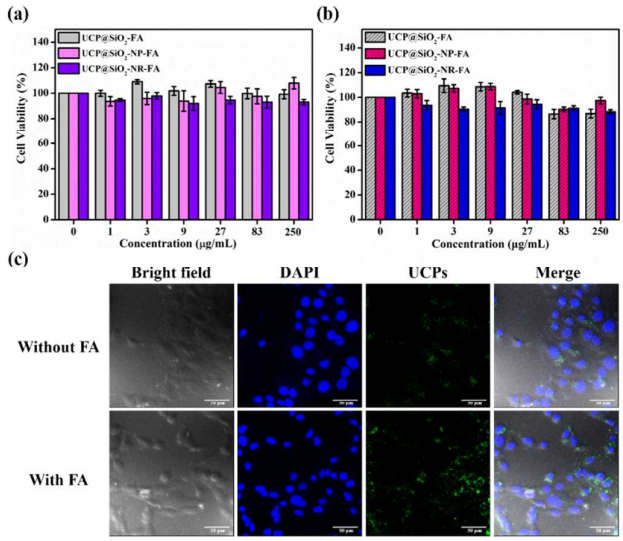

Figure 9. Cell viability of incubating UCP@SiO_2, UCP@SiO_2-NPs-FA and UCP@SiO_2-NRs-FA with OECM-1 for a) 24 and b) 72 h; c) Confocal images of OECM-1 for treating with UCP@SiO_2-NRs and UCP@SiO_2-NRs-FA for 12 h. DAPI were used to stain for marking the location of nucleus.

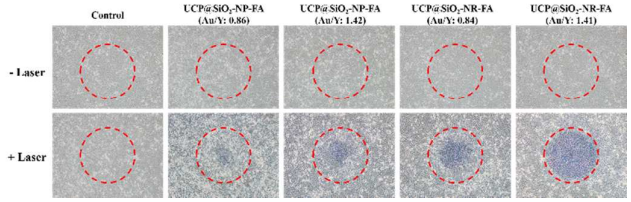

Figure 10. PTT for treating OECM-1 with medium only, UCP@SiO_2-NPs-FA and UCP@SiO_2-NRs-FA with low and high Au/Y ratio for 12 h. The death cell were stained by trypan blue immediately.

4. Conclusions

In this study, we determined the optimal conditions for the combination of UCPs and Au NMs as bifunctional nanocomposites in the treatment of OECM-1 oral cancer cells via PTT and cell imaging. First, UCP@SiO_2-NPs-FA and UCP@SiO_2-NRs-FA were prepared via a multi-step process, and the size, morphology, and crystalline phase of the fabricated nanocomposites were confirmed by TEM, high-resolution TEM and powder XRD. The mechanism and efficiency of energy transfer from UCPs to Au NMs were investigated via characterization of the variation of UCL PL intensity and decay time emission. A simulative model for the Au NP and Au NR systems was used to study the heat quality and heat distribution generated by green and red UCL emissions under laser irradiation at 980 nm. Moreover, in vitro studies showed the non-cytotoxicity of the nanocomposites before exposure to 980 nm laser and revealed an exceptional therapeutic efficiency via photothermal effect. Based on the results, the highly potent nanocomposites for PTT and cell imaging are the UCP@SiO_2-NRs-FA with a 4.3 nm thick silica shell and a 1.41 Au/Y ratio.

In this study, we determined the optimal conditions for the combination of UCPs and Au NMs as bifunctional nanocomposites in the treatment of OECM-1 oral cancer cells via PTT and cell imaging. First, UCP@SiO2-NPs-FA and UCP@SiO2-NRs-FA were prepared via a multi-step process, and the size, morphology, and crystalline phase of the fabricated nanocomposites were confirmed by TEM, high-resolution TEM and powder XRD. The mechanism and efficiency of energy transfer from UCPs to Au NMs were investigated via characterization of the variation of UCL PL intensity and decay time emission. A simulative model for the Au NP and Au NR systems was used to study the heat quality and heat distribution generated by green and red UCL emissions under laser irradiation at 980 nm. Moreover, in vitro studies showed the non-cytotoxicity of the nanocomposites before exposure to 980 nm laser and revealed an exceptional therapeutic efficiency via photothermal effect. Based on the results, the highly potent nanocomposites for PTT and cell imaging are the UCP@SiO2-NRs-FA with a 4.3 nm thick silica shell and a 1.41 Au/Y ratio.

Acknowledgements

The authors would like to thank the Ministry of Science and Technology of Taiwan (Contract No. MOST 104-2113-M-002-012-MY3) and Academia Sinica (Contract No. AS-103-TP-A06) for financially supporting this research. This work is also supported by the NSFC (No. U1305244 and 21325104) and the CAS/SAFEA International Partnership Program for Creative Research Teams. Thanks to Ms. C.Y. Chien of the Precious Instrument Center (National Taiwan University) for the assistance in TEM experiments and Ms. Li-Wen Lo of The Genomics Research Center, Academia Sinica for the help with the confocal microscopy.

Notes and references

[a]Department of Chemistry, National Taiwan University, Taipei 106, Taiwan. E-mail: rsliu@ntu.edu.tw
[b]Genomics Research Center, Academia Sinica, Taipei 115, Taiwan. E-mail: mhsiao@gate.sinica.edu.tw
[c]Department of Mechanical Engineering and Graduate Institute of Manufacturing Technology, National Taipei University of Technology, Taipei 106, Taiwan.
[d]Institute of Microbiology and Immunology, National Yang-Ming University, Taipei 112, Taiwan.
[e]Department of Physics, National Taiwan University, Taipei 10617, Taiwan. E-mail: dptsai@phys.ntu.edu.tw
[f]Research Center for Applied Sciences, Academia Sinica, Taipei 11529, Taiwan.
[g]Key Laboratory of Optoelectronic Materials Chemistry and Physics, Fujian Institute of Research on the Structure of Matter, Chinese

Academy of Sciences, Fuzhou, Fujian 350002, China. E-mail: xchen@fjirsm.ac.cn

Electronic Supplementary Information (ESI) available: TEM images, analytical data and electronic field of UCP@SiO_2-NP and UCP@SiO_2-NR. See DOI: 10.1039/b000000x/

1. P. Wust, B. Hildebrandt, G. Sreenivasa, B. Rau, J. Gellermann, H. Riess, R. Felix and P. M. Schlag, *Lancet Oncol.*, 2002, **3**, 487-497.
2. X. Huang, I. H. El-Sayed, W. Qian and M. A. El-Sayed, *J. Am. Chem. Soc.*, 2006, **128**, 2115-2120.
3. X. Huang, P. Jain, I. El-Sayed and M. El-Sayed, *Lasers Med. Sci.*, 2008, **23**, 217-228.
4. S. Lal, S. E. Clare and N. J. Halas, *Acc. Chem. Res.*, 2008, **41**, 1842-1851.
5. K. König, *J. Microbiol.*, 2000, **200**, 83-104.
6. C. Loo, A. Lowery, N. Halas, J. West and R. Drezek, *Nano Lett.*, 2005, **5**, 709-711.
7. R. Bardhan, S. Lal, A. Joshi and N. J. Halas, *Acc. Chem. Res.*, 2011, **44**, 936-946.
8. N. J. Durr, T. Larson, D. K. Smith, B. A. Korgel, K. Sokolov and A. Ben-Yakar, *Nano Lett.*, 2007, **7**, 941-945.
9. W.-S. Kuo, C.-N. Chang, Y.-T. Chang, M.-H. Yang, Y.-H. Chien, S.-J. Chen and C.-S. Yeh, *Angew. Chem. Int. Ed.*, 2010, **49**, 2711-2715.
10. P. Huang, W. Zheng, S. Zhou, D. Tu, Z. Chen, H. Zhu, R. Li, E. Ma, M. Huang and X. Chen, *Angew. Chem. Int. Ed.*, 2014, **53**, 1252-1257.
11. R. Deng, X. Xie, M. Vendrell, Y.-T. Chang and X. Liu, *J. Am. Chem. Soc.*, 2011, **133**, 20168-20171.
12. C. K. Chen, H. M. Chen, C.-J. Chen and R.-S. Liu, *Chem. Commun.*, 2013, **49**, 7917-7919.
13. N. M. Idris, M. K. Gnanasammandhan, J. Zhang, P. C. Ho, R. Mahendran and Y. Zhang, *Nat. Med.*, 2012, **18**, 1580-1585.
14. M. K. G. Jayakumar, A. Bansal, K. Huang, R. Yao, B. N. Li and Y. Zhang, *ACS Nano*, 2014, **8**, 4848-4858.
15. G.-L. Law, W.-M. Kwok, W.-T. Wong, K.-L. Wong and P. A. Tanner, *J. Phys. Chem. B*, 2007, **111**, 10858-10861.
16. W.-S. Lo, W.-M. Kwok, G.-L. Law, C.-T. Yeung, C. T.-L. Chan, H.-L. Yeung, H.-K. Kong, C.-H. Chen, M. B. Murphy, K.-L. Wong and W.-T. Wong, *Inorg. Chem.*, 2011, **50**, 5309-5311.
17. F. Wang and X. Liu, *Chem. Soc. Rev.*, 2009, **38**, 976-989.
18. F. Auzel, *Chem. Rev.*, 2004, **104**, 139-174.
19. M. M. Lezhnina, T. Jüstel, H. Kätker, D. U. Wiechert and U. H. Kynast, *Adv. Funct. Mater.*, 2006, **16**, 935-942.
20. F. Vetrone, R. Naccache, V. Mahalingam, C. G. Morgan and J. A. Capobianco, *Adv. Funct. Mater.*, 2009, **19**, 2924-2929.
21. S. Schietinger, T. Aichele, H.-Q. Wang, T. Nann and O. Benson, *Nano Lett.*, 2010, **10**, 134-138.
22. H. Zhang, Y. Li, I. A. Ivanov, Y. Qu, Y. Huang and X. Duan, *Angew. Chem. Int. Ed.*, 2010, **49**, 2865-2868.
23. M. Saboktakin, X. Ye, S. J. Oh, S.-H. Hong, A. T. Fafarman, U. K. Chettiar, N. Engheta, C. B. Murray and C. R. Kagan, *ACS Nano*, 2012, **6**, 8758-8766.
24. X. Chen, W. Xu, L. Zhang, X. Bai, S. Cui, D. Zhou, Z. Yin, H. Song and D.-H. Kim, *Adv. Funct. Mater.*, 2015, DOI: 10.1002/adfm.201502419, n/a-n/a.
25. L. Cheng, K. Yang, Y. Li, J. Chen, C. Wang, M. Shao, S.-T. Lee and Z. Liu, *Angew. Chem. Int. Ed.*, 2011, **50**, 7385-7390.
26. B. Dong, S. Xu, J. Sun, S. Bi, D. Li, X. Bai, Y. Wang, L. Wang and H. Song, *J. Mater. Chem.*, 2011, **21**, 6193-6200.
27. L. Qian, L. Zhou, H.-P. Too and G.-M. Chow, *J. Nanopart. Res.*, 2011, **13**, 499-510.
28. Y. Song, G. Liu, X. Dong, J. Wang, W. Yu and J. Li, *RSC Adv.*, 2014, **4**, 62802-62808.
29. F. Wang, R. Deng, J. Wang, Q. Wang, Y. Han, H. Zhu, X. Chen and X. Liu, *Nat. Mater.*, 2011, **10**, 968-973.
30. Z. Li, L. Wang, Z. Wang, X. Liu and Y. Xiong, *J. Phys. Chem. C*, 2011, **115**, 3291-3296.
31. B. Nikoobakht and M. A. El-Sayed, *Chem. Mater.*, 2003, **15**, 1957-1962.
32. J. Ma, P. Huang, M. He, L. Pan, Z. Zhou, L. Feng, G. Gao and D. Cui, *J. Phys. Chem. B*, 2012, **116**, 14062-14070.
33. A. C. Metaxas and R. J. Meredith, *Industrial Microwave Heating*, Institution of Engineering and Technology, 1988.
34. F. Chen, S. Zhang, W. Bu, Y. Chen, Q. Xiao, J. Liu, H. Xing, L. Zhou, W. Peng and J. Shi, *Chem. Eur. J.*, 2012, **18**, 7082-7090.
35. C.-W. Chen, D.-Y. Wu, Y.-C. Chan, C. C. Lin, P.-H. Chung, M. Hsiao and R.-S. Liu, *J. Phys. Chem. C*, 2015, **119**, 2852-2860.
36. D. M. Wu, A. García-Etxarri, A. Salleo and J. A. Dionne, *J. Phys. Chem. Lett.*, 2014, **5**, 4020-4031.
37. M. Ray, T. S. Basu, N. R. Bandyopadhyay, R. F. Klie, S. Ghosh, S. O. Raja and A. K. Dasgupta, *Nanoscale*, 2014, **6**, 2201-2210.
38. R. A. Petros and J. M. DeSimone, *Nat. Rev. Drug Discov.*, 2010, **9**, 615-627.
39. J. Shen, K. Li, L. Cheng, Z. Liu, S.-T. Lee and J. Liu, *ACS Appl. Mater. Interfaces*, 2014, **6**, 6443-6452.

Table of Contents Graphic

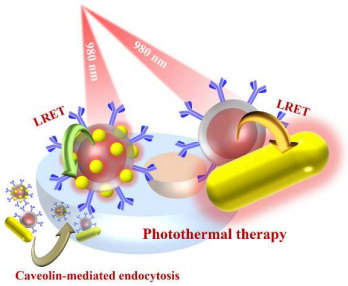

Bi-functional nanocomposites consisting of upconversion nanoparticles and gold nanoparticles or gold nanorods are fabricated for oral cancer cell photothermal therapy.